

AD _____

GRANT NUMBER DAMD17-96-1-6200

TITLE: A Dedicated PET Scanner for Axillary Node Imaging

PRINCIPAL INVESTIGATOR: Simon Cherry, Ph.D.

CONTRACTING ORGANIZATION: University of California, Los Angeles
Los Angeles, CA 90095-1406

REPORT DATE: September 1997

TYPE OF REPORT: Annual

PREPARED FOR: Commander
U.S. Army Medical Research and Materiel Command
Fort Detrick, Frederick, Maryland 21702-5012

DISTRIBUTION STATEMENT: Approved for public release;
distribution unlimited

The views, opinions and/or findings contained in this report are those of the author(s) and should not be construed as an official Department of the Army position, policy or decision unless so designated by other documentation.

UNCLASSIFIED

19980130 171

REPORT DOCUMENTATION PAGE			Form Approved OMB No. 0704-0188	
Public reporting burden for this collection of information is estimated to average 1 hour per response, including the time for reviewing instructions, searching existing data sources, gathering and maintaining the data needed, and completing and reviewing the collection of information. Send comments regarding this burden estimate or any other aspect of this collection of information, including suggestions for reducing this burden, to Washington Headquarters Services, Directorate for Information Operations and Reports, 1215 Jefferson Davis Highway, Suite 1204, Arlington, VA 22202-4302, and to the Office of Management and Budget, Paperwork Reduction Project (0704-0188), Washington, DC 20503.				
1. AGENCY USE ONLY (Leave blank)	2. REPORT DATE September 1997	3. REPORT TYPE AND DATES COVERED Annual (1 Sep 96 - 31 Aug 97)		
4. TITLE AND SUBTITLE A Dedicated PET Scanner for Axillary Node Imaging		5. FUNDING NUMBERS DAMD17-96-1-6200		
6. AUTHOR(S) Simon Cherry, Ph.D.				
7. PERFORMING ORGANIZATION NAME(S) AND ADDRESS(ES) University of California, Los Angeles Los Angeles, CA 90095-1406		8. PERFORMING ORGANIZATION REPORT NUMBER		
9. SPONSORING/MONITORING AGENCY NAME(S) AND ADDRESS(ES) Commander U.S. Army Medical Research and Materiel Command Fort Detrick, Frederick, Maryland 21702-5012		10. SPONSORING/MONITORING AGENCY REPORT NUMBER		
11. SUPPLEMENTARY NOTES				
12a. DISTRIBUTION / AVAILABILITY STATEMENT Approved for public release; distribution unlimited		12b. DISTRIBUTION CODE		
13. ABSTRACT (Maximum 200) A key prognostic factor in breast cancer is the involvement of the axillary lymph nodes. This is currently determined by axillary lymph node dissection (ALND), a low yield surgical procedure associated with significant cost and morbidity. Positron emission tomography (PET), using [F-18]-fluorodeoxyglucose (FDG) tracer is a sensitive and non-invasive test for lymph node involvement and can be a cost-effective alternative to ALND. In this grant, we are developing a low cost, high performance dedicated PET camera for imaging the axillary nodes. This report summarizes the proposed design for the PET camera based on extensive simulation and benchtop detector measurements. The system will consist of two rectangular gamma-ray detectors operated in coincidence, using the new scintillator LSO and is projected to have significantly improved resolution and sensitivity compared with regular clinical PET scanners. We also report on the development of a realistic phantom of the human torso for testing such dedicated PET cameras and show the importance in terms of the impact of scatter and attenuation of using such a realistic phantom. Based on the work in this report, we will now proceed to build and test the prototype PET system.				
14. SUBJECT TERMS Breast Cancer			15. NUMBER OF PAGES 14	
			16. PRICE CODE	
17. SECURITY CLASSIFICATION OF REPORT Unclassified	18. SECURITY CLASSIFICATION OF THIS PAGE Unclassified	19. SECURITY CLASSIFICATION OF ABSTRACT Unclassified	20. LIMITATION OF ABSTRACT Unlimited	

FOREWORD

Opinions, interpretations, conclusions and recommendations are those of the author and are not necessarily endorsed by the U.S. Army.

____ Where copyrighted material is quoted, permission has been obtained to use such material.

____ Where material from documents designated for limited distribution is quoted, permission has been obtained to use the material.

SRC Citations of commercial organizations and trade names in this report do not constitute an official Department of Army endorsement or approval of the products or services of these organizations.


____ In conducting research using animals, the investigator(s) adhered to the "Guide for the Care and Use of Laboratory Animals," prepared by the Committee on Care and Use of Laboratory Animals of the Institute of Laboratory Resources, National Research Council (NIH Publication No. 86-23, Revised 1985).

SRC For the protection of human subjects, the investigator(s) adhered to policies of applicable Federal Law 45 CFR 46.

____ In conducting research utilizing recombinant DNA technology, the investigator(s) adhered to current guidelines promulgated by the National Institutes of Health.

____ In the conduct of research utilizing recombinant DNA, the investigator(s) adhered to the NIH Guidelines for Research Involving Recombinant DNA Molecules.

____ In the conduct of research involving hazardous organisms, the investigator(s) adhered to the CDC-NIH Guide for Biosafety in Microbiological and Biomedical Laboratories.



PI - Signature

9/23/97

Date

TABLE OF CONTENTS

FRONT COVER	1
REPORT DOCUMENTATION PAGE	2
FOREWORD	3
TABLE OF CONTENTS	4
INTRODUCTION	5
RESEARCH REPORT: DETECTOR MEASUREMENTS	6
DATA ACQUISITION SYSTEM	7
SYSTEM SIMULATION AND DESIGN	8
PHANTOM DEVELOPMENT	8
CONCLUSIONS	13
REFERENCES	13
APPENDICES: BIBLIOGRAPHY	14
LIST OF PERSONNEL	14

INTRODUCTION

Axillary lymph node involvement is the most important prognostic factor determining survival in patients with breast cancer. For this reason, virtually all these patients undergo axillary lymph node dissection (ALND), a surgical procedure which allows pathological examination of the nodes [1]. Unfortunately, ALND is associated with high cost and significant morbidity. In women receiving partial mastectomies, it is most commonly performed as a separate procedure, requiring hospitalization, general anesthesia and one to two weeks of post-operative drain care. Complications from this procedure include post-operative seroma formation, arm and breast edema, nerve injuries and shoulder dysfunction.

As a result of the introduction of screening programs and improvements in mammography, many breast cancers are being discovered at an earlier stage, and for this reason, the rate for positive findings during ALND procedures has dropped to as little as 25% [2]. Furthermore, earlier detection and changes in the management of breast carcinoma have resulted in a large increase in the number of women electing breast conservation therapy, where a partial mastectomy is combined with local radiation therapy. Partial mastectomies can be performed on an outpatient basis and do not require hospitalization. The value of an accurate, non-invasive test for axillary lymph node involvement is therefore clear. It would eliminate the need for hospitalization for tens of thousands of women and avoid the costs and morbidity associated with the surgical dissection of the axillary nodes.

Possible non-invasive tests include clinical examination and X-ray computed tomography. Both of these techniques have failed to show the necessary sensitivity to be considered as a replacement to the surgical ALND procedure [1,3-4]. However, a multi-center study using positron emission tomography (PET), with 2-[F-18]-fluoro-2-deoxy-D-glucose (FDG) as the tracer, demonstrated a sensitivity and specificity of 96% [2,5-9]. The average uptake in axillary metastases ranges from 2:1 to 30:1 relative to normal surrounding tissue [5]. These studies were carried out in conventional whole-body PET scanners. The same group showed, using conservative estimates, that by using PET instead of ALND in patients who were candidates for breast conservation therapy, the economic savings would be in excess of 50 million dollars a year. In addition, more than 70,000 women a year would have been spared ALND and its associated complications. These figures are for the United States alone.

Despite this very encouraging data, there are still two barriers which serve to hinder the widespread application of PET as a non-invasive test for axillary lymph node involvement. Firstly, according to the data, 3% of women with axillary node involvement are likely to be misclassified by PET. In general, these will be women who have less extensive lymph node involvement which the current generation of clinical PET scanners lack the sensitivity and spatial resolution to detect. Although this is regarded as an acceptable trade-off, since for every patient misclassified, 33 patients will have been spared the cost and morbidity of ALND, improvements in the sensitivity of PET techniques would be welcomed. A more practical aspect is related to the availability of PET instrumentation itself. Modern clinical PET scanners are extremely expensive and there are only approximately 40 PET scanners in the United States. It is unrealistic that these centers could scan 70,000 patients a year, and the geographic distribution of the scanners does not necessarily reflect the distribution of the patients.

To address both these issues, we are developing a small dedicated PET scanner designed for axillary node imaging. This system is designed to be an order of magnitude cheaper than whole-body clinical PET scanners, thus making the device attractive to smaller hospitals. By designing the system to perform a specific task, we can obtain better resolution and sensitivity compared with conventional clinical PET scanners, which should lead to a reduction in the number of false negative scans compared with current PET technology.

One issue that is often raised when proposing low cost dedicated PET devices is the problem of tracer availability. It has been shown however, that roughly 90% of the hospital beds in the U.S. are within delivery range of FDG [10], the tracer of choice for this application. This means that on-site cyclotrons will not be required for the majority of hospitals wishing to use such a device, further reducing the complexity and costs associated with the study.

Although our original proposal focused on developing a camera for axillary node imaging, the reviewers strongly urged us to try and develop a device that could also be used to image the primary lesions in the breast. We have heeded this advice, and the system we are now proposing is very flexible allowing use for both axillary node and/or breast imaging. In addition, since writing the proposal, significant developments have taken place in PET detector technology as described below, rendering the detectors we proposed to use obsolete. We are therefore taking advantage of this new technology in the prototype system.

In this report, we give a detailed account of our first year of work on this project. We describe our benchtop detector measurements (page 6) and the design of the data acquisition system (page 7), the development of Monte Carlo simulation code (page 8), and the design, realization and testing of a realistic phantom for pre-clinical testing of our system (page 9). These sections represent each of the specific aims for year 1 as outlined in the Statement of Work in the original proposal.

RESEARCH REPORT

Part 1: Detector Measurements

There have been many developments in detector technology for PET over the past two years, initiated, in large part, by the commercial availability of a new scintillator, lutetium oxyorthosilicate (LSO). This scintillator has a similar stopping power to bismuth germanate (the scintillator used in most modern PET systems), but produces approximately five times as much scintillation light and has a seven-fold shorter decay time [11]. This latter property is of extreme importance for the system we are proposing to develop, as it enables us to construct detectors which can operate successfully in high singles count rate environments. Given the difficulty of effectively shielding our detector system, and the proximity during imaging to major organs such as the heart which often takes up significant quantities of ^{18}F -FDG, the use of LSO scintillator in our detectors will result in much improved count-rate performance compared with conventional PET detectors.

The availability of LSO has led us to rethink our detector strategy outlined in the original proposal. Instead of conventional BGO block detectors, we will utilize LSO scintillators mounted onto a position sensitive photomultiplier tube. To prove the feasibility of this approach, we constructed a prototype detector consisting of an 8 x 8 array of LSO crystals (each with dimensions 2 x 2 x 10 mm) coupled by optical fibers to a new, compact, low-cost crossed-wire position sensitive PMT, the Hamamatsu R5900-C8. A similar approach has been successfully employed in a small animal PET [12], although that used a more bulky and expensive multi-channel PMT.

The Hamamatsu R5900-C8 is a crossed wire PMT with 4 wires in the X direction and 4 wires in the Y direction. A simple resistive chain is used to readout the X and Y centroid of the scintillation light which strikes the photocathode of the PMT. Figure 1 shows the output of the prototype detector module after irradiation with a ^{22}Na source. All 64 LSO elements are clearly resolved. Figure 2 shows an energy spectrum from one crystal element when coupled through 12 cm of optical fiber. The mean energy resolution across the detector module is 24%.

The advantages of LSO based detectors are just too great to be ignored for this project and we are in the fortunate position of being able to take advantage of this new material through our technology transfer agreement with CTI PET Systems Inc. These detectors will be made in collaboration with CTI, just as the original BGO block detectors would have been. Sufficient LSO is already on hand to build a prototype imaging system and there will be no significant cost increase by moving to the LSO based detectors. A schematic of the proposed detector module based on LSO scintillator read out by a Hamamatsu R5900-C8 PMT is shown in Figure 3. The final dimensions of the crystal elements and the optical fibers will depend on the outcome of the simulations described below. It is anticipated that the elements will be approximately 2.5 x 2.5 x 15 mm.

Note that the use of short lengths of optical fibers retains the ability to pack detector modules immediately adjacent to each other resulting in detector plates with minimal deadspace which are active and functional right to the very edges. This was a key part of the original proposal and the retention of these advantages was an important consideration in the new detector design.

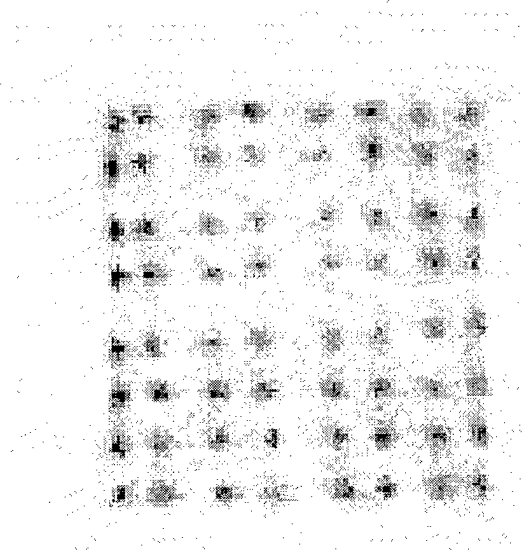


Figure 1: Position histogram for detector module - all 64 crystals are clearly resolved.

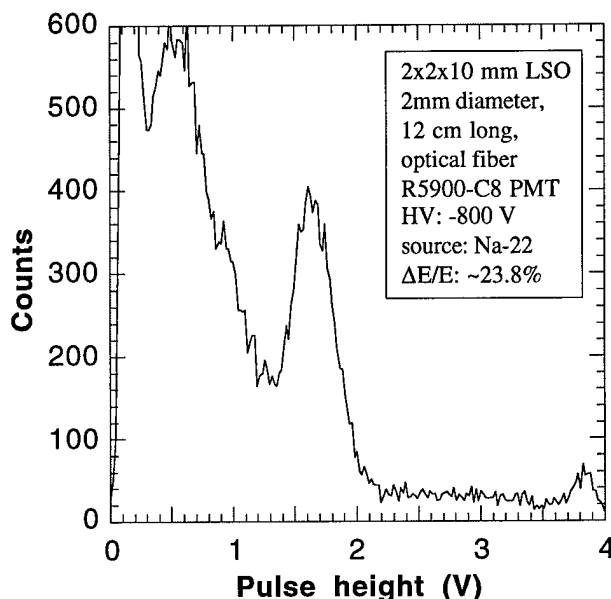


Figure 2: Energy spectrum from detector module. Energy resolution is ~24%.

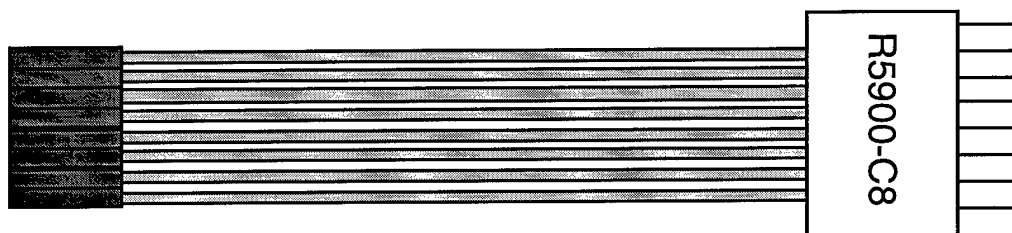


Figure 3: Axillary node imaging with PET: A schematic drawing of the proposed detector module in cross section showing the LSO scintillators (left) coupled by 10 cm of optical fibers into a R5900-C8 position sensitive PMT.

Part 2: Data Acquisition System

We have researched the electronics and data acquisition system for the axillary node imaging PET system. Key factors were flexibility in controlling data acquisition, adequate count rate performance, use of state-of-the-art hardware and low cost. Based on all of these factors, we have purchased the following components for our data acquisition system: 1) A 16 channel amplifier NIM module (C.A.E.N. Model N568) with individual gain adjustment for each channel and variable shaping time; 2) two NIM constant fraction discriminators (Tennelec Model 453) and a NIM quad four-fold logic unit (Philips Scientific Model 755) for determining valid coincidence events between the two detector plates; 3) A 16 channel digitizer PCI board (DATEL PCI-416) with 12-16 bit A/D resolution and approximately 200 kHz rate capability (for all 16 channels); 4) a host PC (MICRON Millennia LXE 200) with a 200 MHz Pentium

processor, 128 MB of RAM and a 4 GB hard disk into which the PCI board will be inserted and onto which list mode data will be stored and 5) LabVIEW software to control the data acquisition process and provide the user interface. The data acquisition set-up is shown schematically in figure 4.

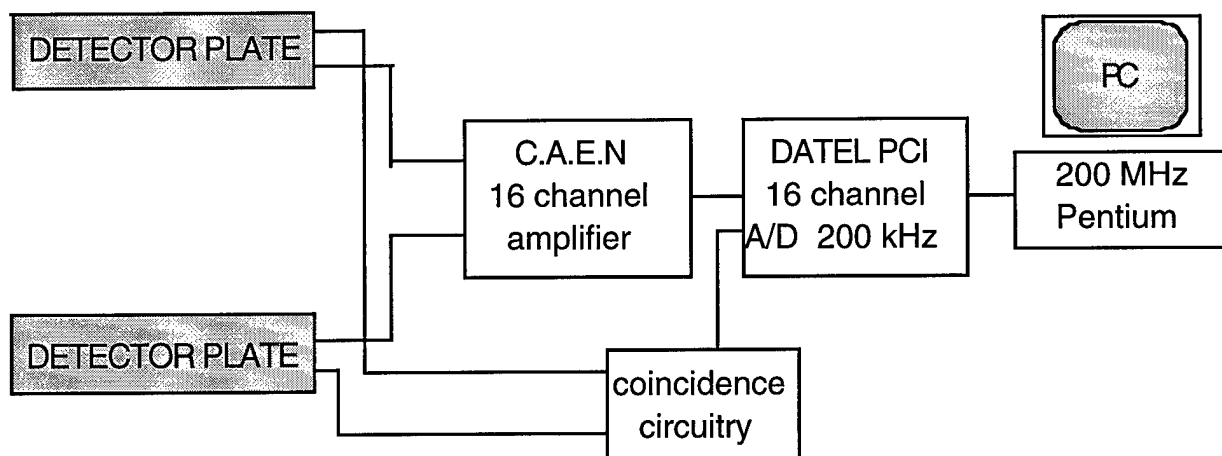


Figure 4: Schematic figure showing electronics to control prototype PET system. All the electronics fit in a small rack, resulting in a compact and mobile system.

Part 3: System Simulation And Design

During year 1 of this grant, we have been actively developing our Monte-Carlo simulation code to simulate different possible PET system geometries for axillary node and breast imaging. There are essentially two options - a small ring of detectors or two planar detector arrays and we have chosen to concentrate on the latter, as we believe this gives us the greatest system flexibility for imaging geometrically complex areas of the body such as the breast and the axillary region. There are several options for how to acquire and reconstruct data from the planar detectors; in static mode either projection images or limited angle reconstructions can be obtained and if the detectors are rotated, fully tomographic images become possible. Other important variables include the detector depth and the separation of the detector arrays (both trade-off system sensitivity with resolution loss due to parallax effects) and the size of the crystal elements within the detector array (governing spatial resolution and cost). The Monte Carlo simulations are an efficient way to examine the multitude of options and will help to optimize the design of the prototype system which will be built during year 2.

Figure 5 shows a flow chart for the Monte-Carlo code that has been developed to date. It allows a great deal of flexibility in defining a lesion within tissue and in defining the detector system to image the lesion. User defined parameters include the size of the lesion, the volume of surrounding tissue, the activity in the lesion, the activity in the background, the location of the lesion within the tissue, the size of the detector plates, the depth of the detector plates, the size of the detector elements within the plate and the separation of the detector plates. This code will enable us to examine the complex trade-offs between system sensitivity, system resolution and system cost and will be invaluable in the design of the prototype system. This Monte-Carlo code is now being tested and validated prior to running the simulations described in the original grant proposal.

Part 4: Phantom Development

Introduction: Before any detector system can be tested on patients, it is vital that it go through stringent pre-clinical testing and a complete performance evaluation. Typically this is done using phantom measurements, where the phantom is a test object which can be filled with radioactivity which is

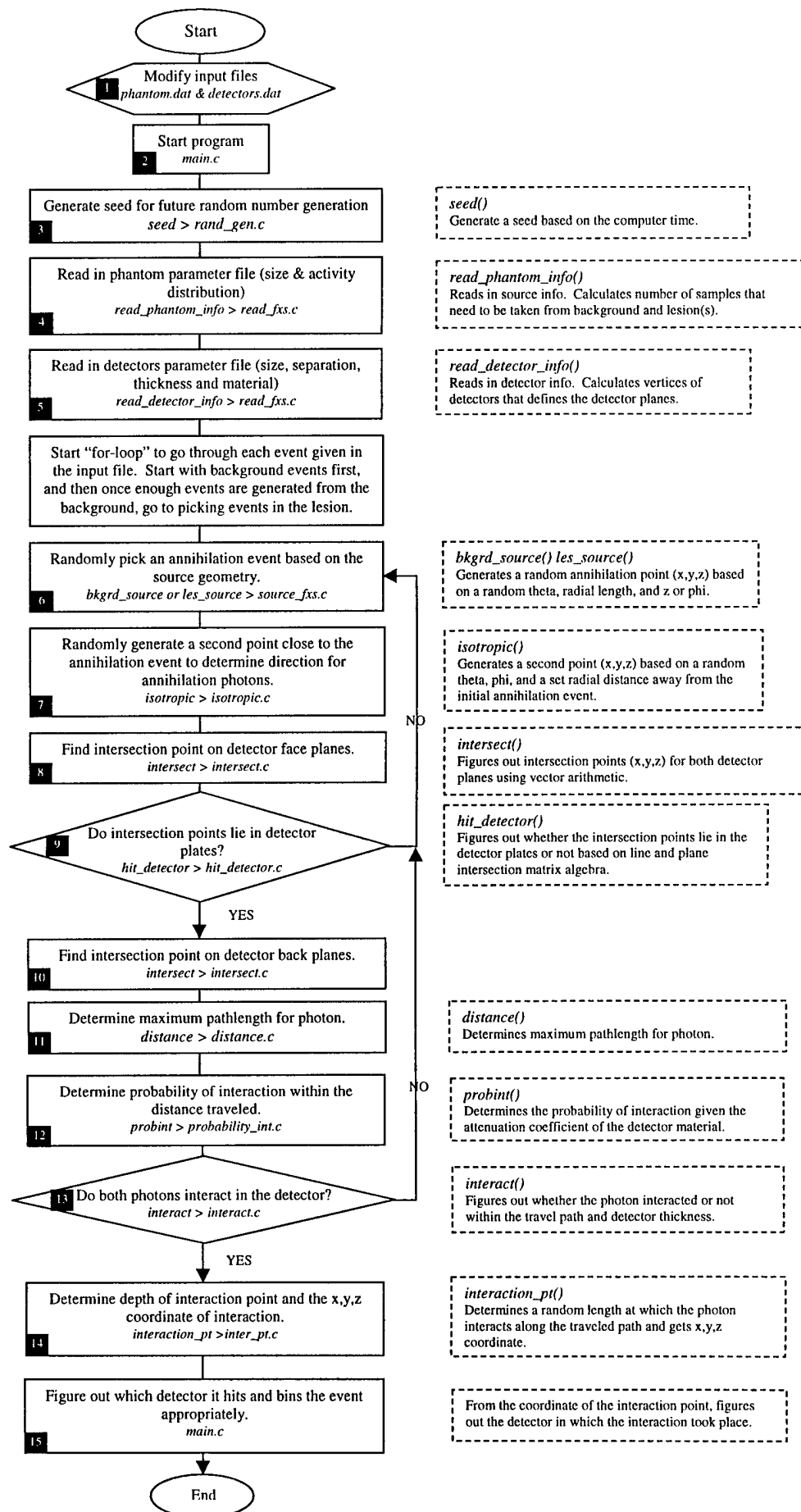


Figure 5: Flowchart for Monte Carlo simulation code.

supposed to represent the imaging situation of interest. To date, most systems designed for imaging in breast cancer have been tested using cylindrical phantoms containing one or more "hot" spheres. We feel strongly, however, that this can be misleading, as the breast and axillary nodes are contained within a geometrically complex region of the body. Activity in the chest, in particular in the heart, leads to a high scattering and high singles to coincidence count rate environment. We have therefore developed a phantom which much more accurately represents this "hostile" imaging environment and have performed a series of experiments to show the importance of using a realistic phantom for pre-clinical testing of imaging devices for breast cancer.

Materials & Methods: In collaboration with Radiology Support Devices Inc. (Long Beach, CA) we have adapted a fully tissue-equivalent anthropomorphic phantom of the human thorax for axillary node and breast imaging. The phantom is constructed with tissue equivalent material with appropriate linear attenuation coefficients. Modifications to the phantom included the addition of channels drilled in the axillary region to allow the simulation of lymph nodes using small capsules containing activity, as well as a set of breast molds in both supine and prone geometry that can be directly attached to the chest with ports for lesions and a cavity for background breast activity. In addition, the phantom contains fillable cavities accurately representing the geometry and location of the heart, liver and thoracic space, allowing simulation of realistic background tissue uptake characteristics. Various sized lesions may be introduced in the breast, axilla, intermammary, and supraclavicular regions to simulate breast cancer patients. The dimensions of the phantom are realistically modeled after humans (see figure 6).

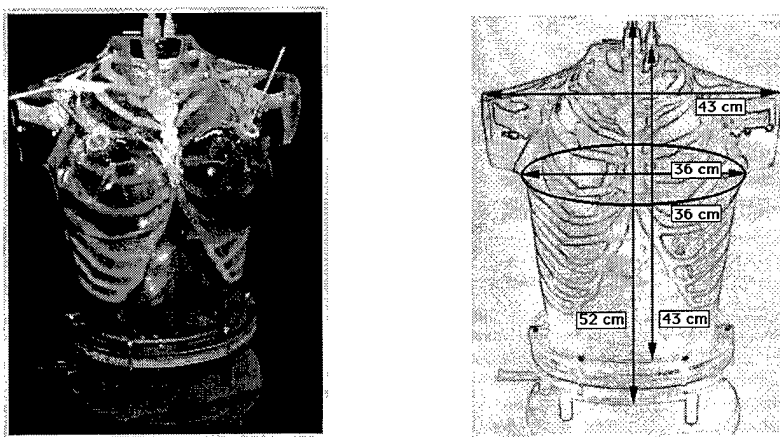


Figure 6: Photograph and schematic representation of anthropomorphic human thorax phantom for simulating breast cancer patients.

Three different experiments were performed on a Siemens/CTI ECAT EXACT HR+ (Knoxville, TN) clinical PET scanner to demonstrate the importance of using an accurate phantom. The experiments were designed to show the role of object scatter, attenuation, and activity distribution in determining signal to noise and contrast in images of the breast.

Experiment 1: In the first experiment, supine geometry breast molds containing single lesions were scanned alone. The left breast was 514 cc containing a 2.55 cc lesion. The right breast was 456 cc and contained a 2.0 cc lesion. The lesion-to-background activities were 7:1 and 5:1 for the left and right breasts, respectively. The activity ratios were verified by taking samples and measuring them in a well counter. The breasts containing the lesions were placed in the supine position during the scanning procedure (figure 7). This setup allowed the closest simulation of a simple phantom, where the scatter and attenuation from the rest of the thorax is ignored. Also, the activity distribution is minimized to that of only the breasts and lesions alone, ignoring the thorax itself and the rest of the organs contained within.



Figure 7. The picture on the left shows the breasts and lesions in the supine position in the gantry of the PET scanner as scanned in experiment 1. The picture on the right shows the position of the phantom as scanned in experiments 2 and 3.

Experiment 2: In experiment 2, the same breast molds and lesions utilized in experiment 1 were now attached to the rest of the thorax. The thorax contained the lungs, heart, and liver and was filled with cold water without any radioisotope. Again, the phantom was placed in the supine position in the scanner as shown in figure 7. In this protocol, an assessment of the contribution of attenuation and scatter only due to the presence of the thorax and its respective organs could be made. The activity distribution remained identical to that in experiment 1.

Experiment 3: In experiment 3, the thoracic cavity, heart, and liver were now all filled with realistic activity concentrations. This scanning setup provided the most complex and closest simulation to that which occurs while scanning a real patient. Thus, in this protocol, the complex geometry, attenuation, scatter and activity distribution were all replicated as closely as possible to a real human's characteristics.

In order to fill the phantom and its various components with realistic activity levels, several breast cancer patient scans from whole-body PET studies were obtained to extract the appropriate data. Regions-of-interest (ROIs) were drawn around the various tissues of interest such as the breast lesion, breast tissue, heart, liver, and background thoracic cavity using a commercially available software package (Clinical Applications Programming Package (CAPP), Siemens/CTI, Knoxville, TN). The ROI values were then converted to activity concentrations in units of microCuries per cubic centimeter for each tissue or organ and are presented in table 1.

Table 1. Concentration values for the various tissues as determined from real patient data.

Tissue/Organ	Concentration (mCi/cc) \pm Std. Dev.
Lesion	0.18 \pm 0.02
Myocardium	0.13 \pm 0.02
Liver	0.11 \pm 0.007
Breast	0.05 \pm 0.006
Thoracic cavity	0.05 \pm 0.006

All the experiments followed a similar scanning protocol. The phantom was filled with ^{18}F -FDG solution as described for each experiment, based on the values in table 1. A 2-D PET scan was acquired with the breasts centered within the 15 cm axial field-of-view (FOV) and the phantom in a supine position. A 60 minute emission scan was taken right after all the components of the phantom were filled and assembled together. A 20 minute transmission scan was taken without the phantom being moved, the following morning, allowing all of the activity to have decayed more than 5 half-lives. Filtered backprojection was used for reconstructing the 63 image planes using a Shepp filter with a cutoff frequency equal to 1/2 the

Nyquist frequency. No axial smoothing was performed on the images. All scans were performed on the same scanner and we maintained identical scanning conditions for each experiment.

Results: The resulting images were analyzed using the CAPP software. ROI's were defined over the lesion and over background breast tissue. The signal-to-noise (SNR) was assumed to be proportional to the quotient of the mean ROI values of the lesion divided by the mean of the standard deviations of the background tissue ROI. The lesion ROIs were drawn on all the planes that contained lesion activity in such a fashion as to include all pixels containing at least 70% of the maximum pixel value. The background tissue ROIs were drawn on several planes of the image volume not containing any lesion activity, usually ten planes above the beginning of the lesion activity. The contrast was calculated by taking the mean ROI value for the lesion minus the mean ROI value of the background, then dividing by the mean ROI value for the lesion. Again, the same procedure for ROI drawing was used.

Figure 8 shows reconstructed images of relevant planes for each of the three experiments. One can readily see the differences in image quality due to the variation in attenuation, scatter, and activity distribution between the experimental setups as one moves from left (low scatter, no activity outside of breasts) to right (full scattering from thorax, activity in all organs). Figure 9 shows the calculated SNR and contrast values in each experiment. The numbers confirm the trends seen visually in the images.

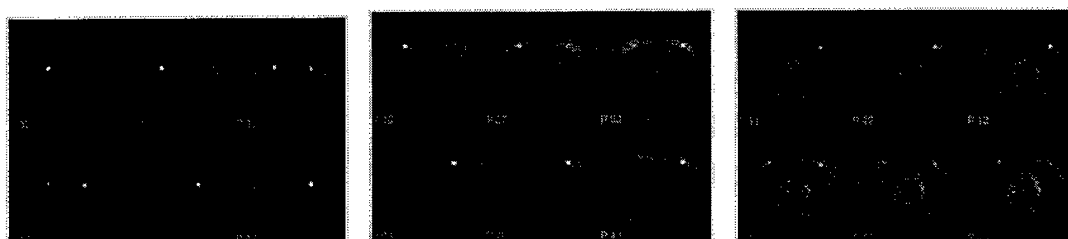


Figure 8. Images from experiment 1 (left - imaging breasts and lesions only), experiment 2 (middle - breasts and lesions attached to water-filled thorax) and experiment 3 (right - breasts and lesions attached to activity filled thorax). Note the change in image quality, even though the amount of radioactivity in the breast and lesions is constant through all three experiments

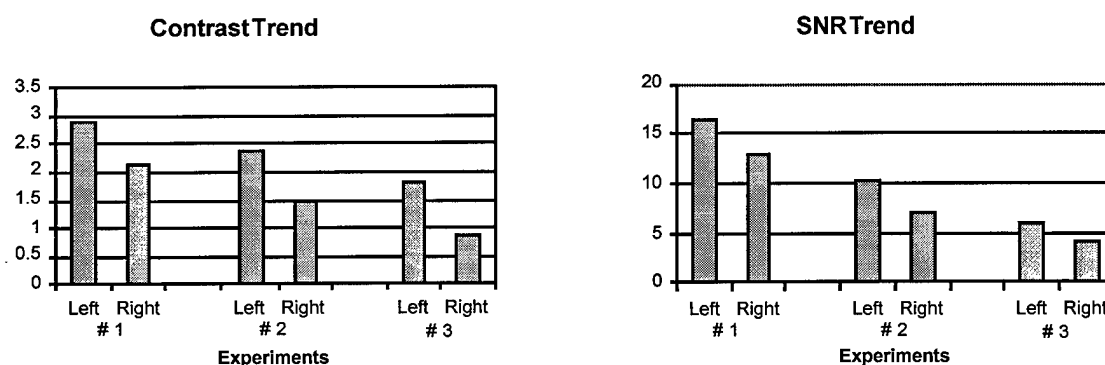


Figure 9. Graphs of the contrast and SNR trends for each of the three experiments. As scattering material and activity outside of the breasts are added, both the contrast and signal-to-noise deteriorate dramatically.

Discussion: These experiments clearly indicate the role of attenuation, scatter and activity outside of the breast in determining image quality. Simple phantoms are likely to be insufficient when comparing imaging systems for applications in breast cancer, because they may not expose the limitations of the imaging system when operated in a hostile imaging environment. This phantom provides a way to accurately assess and optimize the performance of PET systems designed for imaging the breast and axillary nodes and will be an invaluable tool in the development and pre-clinical testing of the device currently under construction at UCLA.

Part 5: Conclusions

We have met the specific aims for year 1 as outlined in the original proposal. The simulation code is almost completed, the phantom has been built and tested and the data acquisition and detector system has been designed and many of the components purchased. We have also built and tested a single LSO detector module. The critical parameters still to be determined are the size of the scintillator elements to be used in each detector plate. This is a trade-off between resolution, sensitivity and cost. The Monte-Carlo simulations and input from our clinical colleagues will guide us in this decision. The Monte-Carlo simulations will also be used to look at different possible reconstruction strategies.

We have not yet encountered any significant difficulties in this work. The biggest challenge has been to adapt the original proposal to take advantage of changes in PET detector technology and electronics which have occurred since the original proposal was written. We believe what we have proposed will give us a much better system at a very similar cost and does not compromise any of the advantages of our original approach. In our opinion we are well on course for building and performing pre-clinical testing of a prototype PET imaging device by the end of year 2.

REFERENCES

1. Danforth DN. The role of axillary lymph node dissection in the management of breast cancer. *Principles and Practices of Oncology* 6: 1-16 (1992).
2. Institute for Clinical PET. Clinical application and economic implications of PET in the assessment of axillary lymph node involvement in breast cancer: a retrospective study. Publication No. CE-BREAST-94.001
3. Logager VB et al. The limited value of routine chest X-ray in the follow up of stage II breast cancer. *Eur J Cancer* 26: 553-555 (1990).
4. March DE et al. CT-pathologic correlation of axillary lymph nodes in breast carcinoma. *J Comput Assist Tomogr* 15: 440-44, 1991.
5. Niewig OE, Kim EE, Wong WH et al. Positron emission tomography with fluorine-18-deoxyglucose in the detection and staging of breast cancer. *Cancer* 71: 3920-25 (1993).
6. Adler LP, Crowe JP, Al-Kaisi NK, Sunshine JL. Evaluation of breast masses and axillary lymph nodes with [F-18] 2-deoxy-2-fluoro-D-glucose PET. *Radiology* 187: 743-750 (1993).
7. Tse NY, Hoh CK, Hawkins RA et al. The application of positron emission tomographic imaging with fluorodeoxyglucose to the evaluation of breast disease. *Ann Surg* 216: 27-34 (1992).
8. Hoh CK, Hawkins RA, Glasby J et al. Cancer detection with whole-body PET using 2-[F-18]-fluoro-2-deoxy-D-glucose. *J Comput Assist Tomogr* 17: 582-589 (1993).
9. Wahl RL, Cody RL, Hutchins GD, Mudgett EE. Primary and metastatic breast carcinoma: initial clinical evaluation with PET and the radio labeled glucose analog 2-[F-18]-fluoro-2-deoxy-D-glucose. *Radiology* 179: 765-70 (1991).
10. Ronald Nutt, CTI PET Systems Inc. Personal Communication
11. Melcher CL, Schweitzer JS. Cerium-doped lutetium oxyorthosilicate: a fast, efficient new scintillator. *IEEE Trans Nucl Sci* 39: 505-505 (1992).
12. Cherry SR, Shao Y, Silverman RW, Chatziioannou A, Meadors K, Siegel S, Farquhar T, Young J, Jones WF, Newport D, Moyers C, Andreaco M, Paulus M, Binkley D, Nutt R, Phelps ME. MicroPET: a high resolution PET scanner for imaging small animals. *IEEE Trans Nucl Sci* 1997; 44: 1161-1166.

APPENDIX A: BIBLIOGRAPHY

Doshi NK, Basic M, Cherry SR, Pang LJ. Development of a realistic multimodality breast and axillary node phantom. J Nucl Med 38: 203P 1997 (presented at the 44th Annual Meeting of the Society of Nuclear Medicine, San Antonio, May 1997).

Shao Y, Cherry SR, Boutefnouchet A, Silverman RW, Majewski S, Wojcik R, Weisenberger AG. Evaluation of Hamamatsu R5900-M16 multi-anode PMT for readout of scintillator arrays. To be presented at the 1997 IEEE Medical Imaging Conference, Albuquerque, NM, November 1997.

Boutefnouchet A, Majewski S, Cherry SR, Shao Y, Silverman RW, Meadors K, Slates R. Possibility for a very high resolution LSO PET detector based on the 16-channel R5900-M16 PMT. To be presented at the 1997 IEEE Medical Imaging Conference, Albuquerque, NM, November 1997.

Doshi NK, Basic M, Cherry SR. Development of a realistic multimodality breast and axillary node phantom. J Nucl Med (in preparation)

APPENDIX B: LIST OF PERSONNEL:

The following personnel were paid in part from this grant:

Niraj K. Doshi

Simon R. Cherry

Sanjiv Gambhir

Erkan U. Mumcuoglu